Research Article

Nano Research
2023, 16(2): 2808–2820

ISSN 1998-0124 CN 11-5974/O4
https://doi.org/10.1007/s12274-022-4947-5

Gadolinium-containing semiconducting polymer nanoparticles for magnetic resonance/fluorescence dual-modal imaging and photothermal therapy of oral squamous cell carcinoma

Xiao Pan[1,§], Antian Gao[1,§], Yanni Hu[1], Ziyang Hu[1], Chen Xie[2] (✉), and Zitong Lin[1] (✉)

[1] *Department of Dentomaxillofacial Radiology, Affiliated Stomatology Hospital of Medical School, Nanjing University, Nanjing 210008, China*
[2] *Key Laboratory for Organic Electronics and Information Displays & Jiangsu Key Laboratory for Biosensors, Institute of Advanced Materials (IAM), Jiangsu National Synergetic Innovation Center for Advanced Materials (SICAM), Nanjing University of Posts & Telecommunications, Nanjing 210023, China*
[§] *Xiao Pan and Antian Gao contributed equally to this work.*

Received: 22 June 2022 / **Revised:** 22 August 2022 / **Accepted:** 23 August 2022

ABSTRACT

Oral squamous cell carcinoma (OSCC) is the most common malignant tumor of the oral and maxillofacial region. Due to its unique location, earlier and more accurate diagnosis and more minimally invasive treatment of OSCC is of major importance. Herein, gadolinium-containing semiconductor polymer nanoparticles (SPN-Gd) were designed and prepared. The nanoparticles consist of a near-infrared (NIR) absorption semiconductor polymer (PCPDTBT) served as fluorescence signal source and a photothermal conversion agent (PTA) and a gadolinium-grafted triblock amphiphilic copolymer (F127-DTPA-Gd) served as a magnetic resonance imaging (MRI) contrast agent and nanocarrier. The experiments *in vivo* showed that SPN-Gd could act as an MRI contrast agent and optical image agent with a long retention time, and it had a significant inhibiting effect on tumors of OSCC mice model through photothermal therapy (PTT). Thus our study provides a simple nanotheranostic platform composed of two components for efficient MR/fluorescence dual-modal imaging-guided PTT.

KEYWORDS

oral squamous cell carcinoma, magnetic resonance imaging, fluorescence imaging, dual-modal imaging, photothermal therapy, semiconducting polymer nanoparticles

1 Introduction

Oral squamous cell carcinoma (OSCC) is the most common type of cancer in the head and neck area [1, 2]. It is among the most common malignant tumors, with approximately 370,000 new cases diagnosed annually worldwide, causing about 180,000 deaths [3, 4]. Despite the advancements of diagnostics and therapeutics, the five-year survival rate has not significantly improved in recent years. Moreover, due to the special location of OSCC, radical surgical resection and radiotherapy could cause great structural and functional damage and significantly reduce the quality of life of patients. Therefore, earlier and more accurate diagnosis and more minimally invasive treatment of OSCC is essential and has attracted great deal of attention.

Magnetic resonance imaging (MRI), capable of providing high resolution three-dimensional images of soft tissues, has proven useful in the OSCC diagnosis [5]. Although MRI provides much previse images for tumor detection and localization than computed tomography (CT), its signal-to-noise ratio is not always satisfactory. In order to increase the diagnosis sensitivity, MRI contrast agents are widely used clinically for better contrast differences between normal and abnormal tissues [6, 7]. Currently available, gadolinium (Gd^{3+}) chelates are widely used as magnetic resonance T_1 contrast agents due to the fact that Gd^{3+} is an ideal proton relaxation candidate. The prominent position of the Gd^{3+} ion relies not only in a high magnetic moment (7.9 BM) given by seven unpaired electrons in the 4f shell, but also in a totally symmetric electronic state ($8S_{7/2}$ ground state), which makes Gd^{3+} strongly paramagnetic with a much longer electronic relaxation time than other ions [8]. Current Gd-based contrast agents (GBCAs) have advantages in tumour and vascular imaging [9, 10], but as small molecules, GBCAs have a short circulation time and are not tumor specific. The relatively low sensitivity, limited spatial resolution, and difficulties in monitoring treatment are the main disadvantages of current MRI imaging. Gd-based nanoparticles showed promising potential, and they have been approved by the Food and Drug Administration (FDA) for MRI imaging in cancer patients and found to have potential to improve tumor diagnosis [8].

Optical imaging has been gaining increasing attention in tumor diagnosis for its excellent sensitivity, high spatial and temporal resolution, and low experimental cost [11–13]. Semiconducting polymer nanoparticles (SPNs), as a novel category of optical nanomaterials, have been widely applied in the field of bioimaging by virtue of their excellent photostability, high absorption coefficient, and good biocompatibility [14–16]. SPNs with high fluorescence quantum yields are suitable for fluorescence imaging.

Address correspondence to Zitong Lin, linzitong_710@163.com; Chen Xie, iamcxie@njupt.edu.cn

However, as an optical imaging technique, fluorescence imaging is limited by its insufficient detection depth. To overcome the drawbacks of different imaging modalities, multi-model nanoparticles capable of providing multiple types of medical images have attracted extensive research attention [15]. Dual-model MR/fluorescence nanoparticles are one of the most potential for its high sensitivity, accurate localization, and low cost.

Moreover, some optical biomaterials (including SPNs) have high photothermal conversion efficiencies, and can be used for photothermal therapy (PTT) [15, 17]. PTT, as a non-invasive and localized tumor treatment modality, relies on photothermal conversion agents (PTAs) to generate sufficient heat under near-infrared (NIR) light irradiation for treatment [18]. In contrast with traditional treatments, the advantages of PTT include minimal invasiveness, reduced side effects, and high specificity [18]. In addition, PTT can exhibit great selectivity with minimal side effects, since the laser irradiation parameters (e.g., location, laser wavelength, irradiation time, and light intensity) can be precisely controlled. OSCC, as a local and superficial tumor in the oral and maxillofacial region, is suitable for PTT because of its minimal invasive, low side effects, and clinic operability.

Therefore, in this study, in order to overcome the shortcomings of current MRI imaging and fluorescence imaging, to explore a simple and minimally invasive treatment of OSCC, and to develop a theranostic platform for OSCC, a gadolinium-containing semiconducting polymer nanoparticle (SPN-Gd) was designed and prepared. The nanoparticles are composed of a NIR absorption semiconductor polymer (PCPDTBT) served as fluorescence signal source and a PTA and a gadolinium-grafted triblock amphiphilic copolymer (F127-DTPA-Gd) served as an MRI contrast agent and nanocarrier (Fig. 1(a)). In the following, we first described the synthesis of SPN-Gd, followed by the characterization of the nanoparticles and the assessment of their optical properties. Finally, the experimental application of MR/fluorescence dual-modal imaging guided PTT was demonstrated in OSCC tumor bearing mice (Fig. 1(b)).

2 Experimental section

2.1 Materials

Pluronic F127 (M_W = 12,600), diethylenetriamine pentaacetic acid bis-anhydride (DTPA-BA), gadolinium(III) chloride hexahydrate ($GdCl_3 6H_2O$), 1-(3-dimethylaminopropyl)-3-ethylcarbodiimide hydrochloride (EDC), 4-dimethylaminopyridine (DMAP), and dimethyl formamide (DMF) were purchased from J&K Scientific Co., Ltd. (Shanghai, China). Poly[2,6-(4,4-bis-(2-ethylhexyl)4H-cyclopenta[2,1-b;3,4-b']-dithiophene)-alt-4,7-(2,1,3-benzothiadiazole)] (PCPDTBT), red blood cell lysis buffer, and chloral hydrate solution were purchased from Sigma-Aldrich (Shanghai, China). Tetrahydrofuran (THF) was purchased from Aladdin Reagent Co., Ltd. (Shanghai, China). Phosphate buffer saline (PBS) buffer and 0.05% trypsin were purchased from Hyclone (USA); Roswell Park Memorial Institute-1640 Medium (RPMI-1640), high glucose Dulbecco's modified Eagle's medium (DMEM/High), and fetal bovine serum (FBS) were purchased

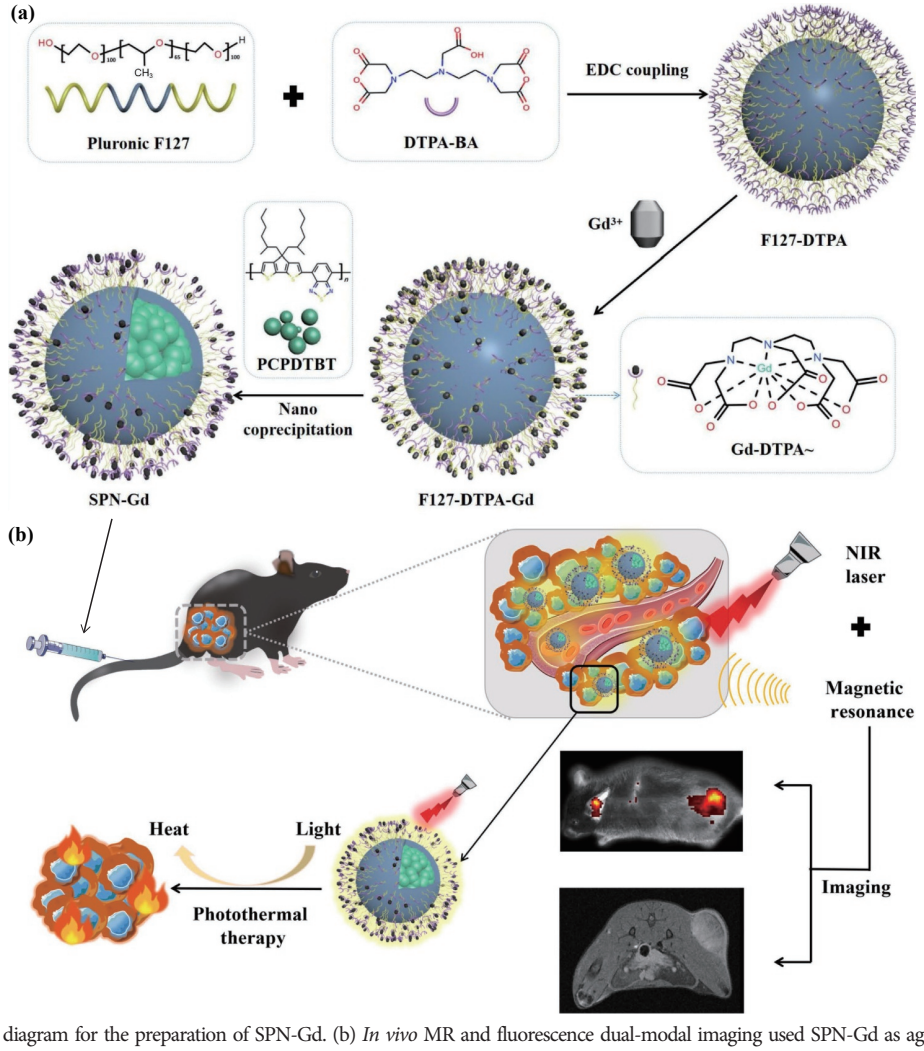

Figure 1 (a) Schematic diagram for the preparation of SPN-Gd. (b) *In vivo* MR and fluorescence dual-modal imaging used SPN-Gd as agent and SPN-Gd-guided photothermal therapy.

from GIBICO (USA). Cell counting kit-8 cell (CCK8) counting reagent was from Titan Scientific Co., Ltd. (Shanghai, China). 4% paraformaldehyde and 4',6-diamidine-2'-phenylindole dihydrochloride (DAPI) were purchased from Beyotime Biotechnology Co., Ltd. (Shanghai, China). PerCP anti-mouse CD45 antibody, FITC anti-mouse CD3 antibody, APC anti-mouse CD4 antibody, and PE anti-mouse CD8a antibody were purchased from BioLegend Co., Ltd. (USA). All reagents were obtained from commercial suppliers and used without further purification. Other commonly used chemical reagents were provided in the laboratory.

2.2 Synthesis of F127-DTPA-Gd

At first, F127-DTPA was prepared using an EDC coupling reaction. The specific steps were as follows. F127 (500 mg), DTPA-BA (141 mg), and DMAP (10 mg) were dissolved in DMF (5 mL), then EDC (75 mg) was added, and the mixture was stirred at room temperature for 48 h. After 48 h, the reaction product was filtered, and the solution was placed in a dialysis bag (molecular weight cut-off = 3,500 DA), dialyzed in deionized water for 24 h to remove small molecular impurities, and the product F127-DTPA was further obtained by lyophilization. The resulting product was prepared by chelation reaction to prepare F127-DTPA-Gd. F127-DTPA (100 mg) and excess $GdCl_3 6H_2O$ (40 mg) were dissolved in deionized water and stirred at room temperature for 24 h. The resulting solution was subsequently placed in a dialysis bag (molecular weight cut-off = 3,500 DA). Free Gd^{3+} and other impurities were removed by dialysis against deionized water for 24 h, and the final product F127-DTPA-Gd was obtained by lyophilization.

2.3 Preparation of semiconducting polymer nanoparticles, SPN-Gd

The MR/fluorescence dual-modal imaging nanoparticles SPN-Gd were prepared by the nanoprecipitation method. F127-DTPA-Gd (50 mg) and PCPDTBT (250 μg) were dissolved in THF (1 mL), and then the solution was quickly injected into THF (2 mL) and deionized water (18 mL) under sonication in a water bath for 2 min. The solution was placed in a dark environment, and nitrogen gas was used to continuously blow the solution to accelerate the evaporation of THF. After all THF in the solution was removed, a filter with a pore size of 0.22 μm was used to remove impurities. Then, the solution was concentrated by ultrafiltration using an ultrafiltration centrifuge tube (molecular weight cut-off = 100,000 DA, rotation speed = 3,500 rpm, time 10 min), and then the SPN-Gd was stored in a 4 °C refrigerator for later use.

2.4 Characterization of nanoparticles

2.4.1 Gd^{3+} ion content, morphology, and diameter

The metal element Gd^{3+} in the nanoparticles was determined by inductively coupled plasma emission spectrometer (PE Company, Avio500, USA). Dynamic light scattering nano Laser Particle Sizer (DLS, Dandong Baite Instrument Co., Ltd., BT-90, China) and transmission electron microscope (TEM, Japan Electronics Co., Japan) were used to determine the morphology, diameter, and stability of nanoparticles.

2.4.2 Relaxation rates of SPN-Gd

The T_1, T_2-weighted images of SPN-Gd were measured by magnetic resonance (Bruker, BioSpec 94/20 USR, Germany) with a field strength of 9.4 T at 25 °C, respectively. The solutions of F127-DTPA-Gd, SPN-Gd, and Omniscan were prepared in a concentration gradient of 0, 0.05, 0.1, 0.2, and 0.4 mM (calculated as Gd^{3+}) and sealed in 0.6 mL centrifuge tubes and were put into the magnetic resonance. The specific parameters were set as follows: field of view 32 mm × 32 mm, voxel 256 × 256, resolution 0.125 mm, and slice thickness 1.0 mm. The T_1 rare pulse sequence was used to keep the echo time (T_E) at 8.0 ms, and the repetition time (T_R) was: 150, 400, 700, 1,200, 2,000, and 5,000 ms, respectively. Quantitative T_1 relaxation maps were reconstructed from the dataset and T_1 values were measured for each sample. The T_2 value was measured by Turbo rare sequence, the fixed T_R was 2,500 ms, and the T_E was: 7.6, 15.1, 22.7, 30.2, 37.8, 45.4, 52.9, 60.5, 68.0, and 75.6 ms. The data was then measured and the relaxation rates r ($mM^{-1}·S^{-1}$) of the three sets of samples were calculated using the ParaVision 360 workstation. The equation was as follows

$$\left(\frac{1}{T_i}\right)_{obs} = \left(\frac{1}{T_i}\right)_{d} + r_i[M]$$

$(1/T_i)_{obs}$ was the inverse of the proton relaxation time in the presence of magnetic substances, $(1/T_i)_d$ was the inverse of the proton relaxation time in the presence of non-magnetic substances, and $[M]$ was the concentration of magnetic substances. The longitudinal relaxation rates r_1 and transverse relaxation rates r_2 of F127-DTPA-Gd, SPN-Gd, and Omniscan were calculated respectively under 9.4T magnetic resonance.

2.4.3 Optical performance of SPN-Gd

The absorption spectrum was measured by ultraviolet–visible (UV–Vis) spectrophotometer (PerkinElmer, LAMBDA 365, USA). Fluorescence spectra were measured by a fluorescence spectrophotometer (PerkinElmer, FL6500, USA). The content of photosensitizer PCPDTBT in nanoparticles was determined by measuring Abs690 (absorbance (Abs) of about 690 nm) with UV–Vis spectrophotometer. The drug entrapment efficiency (EE) was calculated using this equation

$$\text{EE}\ (\%) = \frac{\text{amount of PCPDTBT in nanoparticles}}{\text{total amount of feeded PCPDTBT}} \times 100\%$$

SPN-Gd (PCPDTBT = 0.04 mg/mL) and ICG (0.04 mg/mL) with the same effective concentration were excited by 808 nm diode laser (Changchun new industry photoelectric technology Co., Ltd., China), and the NIR laser of 1.0 W/cm^2 was used. After 5 min, the absorbance changes of them were measured by fluorescence spectrometer until the absorbance of one of them was close to zero.

At the initial temperature of 25 °C, (1) the SPN-Gd solution (SPN-Gd = 0, 40, 60, 100, 125, and 250 μg/mL) was continuously irradiated with a near-infrared laser of 1.0 W/cm^2 for 5 min, (2) 100 μg/mL SPN-Gd solution was irradiated continuously with different power near-infrared lasers (0.5, 1, and 1.5 W/cm^2) for 5 min, and (3) 100 μg/mL of SPN-Gd solution was irradiated with 1.0 W/cm^2 NIR laser to obtain the heating and cooling curve. For each time, the solution was irradiated for 5 min, and then the solution was cooled until the temperature reached 25 °C; for each solution, the operation was repeated for 3 times. The temperature of SPN-Gd at different time points was recorded by infrared thermal imager (Philip, USA). The SPN-Gd solution temperature was recorded every 10 s.

2.5 Cell cultures

OSCC cell lines SCC7 in C3H/HeJ mouse genetic background cells were cultured in RPMI-1640 medium with 10% FBS at 37 °C in a humidified atmosphere containing 5% CO_2 and 95% air. The mouse embryonic fibroblast lines NIH 3T3 in mouse genetic

background cells were cultured in DMEM/High medium containing 10% FBS at 37 °C in a humidified atmosphere containing 5% CO_2 and 95% air.

2.6 Cellular uptake studies *in vitro*

SCC7 cells in logarithmic growth phase were seeded in confocal small dishes (ϕ35 mm), 10,000 cells per dish, and 2 mL of complete medium was added to culture at 37 °C. After 24 h, cells were washed and added to complete medium containing SPN-Gd (10 μg/mL of SPN-Gd), and incubated in the dark for 30 min and 2 h, respectively. The medium was aspirated at a given time point and the cells were washed repeatedly with PBS, then 4% paraformaldehyde was added to fix the cells for about 10 min; the paraformaldehyde was aspirated, the cells were washed repeatedly with PBS, a total of 170 μL of DAPI staining solution was added, and incubated at room temperature for 10 min. Finally, the DAPI staining solution in the small dish was sucked out, washed with PBS repeatedly, and photographed with a confocal microscope (Nikon Company, Nikon-Eclipse-Ti, Japan).

2.7 Cell viability and apoptosis assays *in vitro*

The biological toxicity of nanoparticles was tested using CCK8. NIH 3T3 cells were seeded in 96-well plates at a cell density of 8,500–10,000 cells per well and added with 100 μL of DMEM/High medium. A blank control group containing the same volume of DMEM/High medium was set for each experiment. The 96-well plate was incubated overnight at 37 °C until cells adhere. Cells were then washed with PBS and incubated with serial dilutions of SPN-Gd (0, 10, 20, 40, 80, and 100 μg/mL) in culture medium, respectively. Incubate for 24 h in the dark at 37 °C and 5% carbon dioxide. After washing the cells in each well with PBS, the nanoparticle-free medium was re-added. Protected from light, 10 μL of CCK8 was gently added to each well and incubated at 37 °C for 1 h. The Abs of each well at a wavelength of 450 nm was then measured every 30 min using a microplate reader (Molecular Devices, SpectraMAX M3, USA) until the Abs value of all wells was 1.0–2.0 and recorded.

SCC7 cells were seeded in 96-well plates at a cell density of 5,500–6,500 cells per well and 100 μL of complete medium was added. A blank control group containing the same volume of complete medium was set for each test. The 96-well plate was incubated at 37 °C overnight until cells adhere. Cells were then washed with PBS and incubated with serially diluted F127-DTPA-Gd, SPN-Gd, and Omniscan (0, 20, 40, 80, 160, and 320 μM, calculated as Gd^{3+} concentration) in complete medium, respectively. Incubate for 24 h at 37 °C in a 5% carbon dioxide environment in the dark. Nanoparticle-free medium was re-added after washing each well of cells with PBS. The others were the same as the above procedures.

In order to further confirm the photothermal cytotoxicity of SPN-Gd on SCC7 cells, the cells were co-incubated with SPN-Gd (0, 10, 20, 40, 80, and 100 μg/mL) at 37 °C for 24 and 48 h and then compared. After that, the mixture was exposed to 808 nm NIR laser irradiation (1.0 W/cm^2) for 5 min. The cells without any treatment or irradiation were set as the control group. The others were the same as the above procedures. Finally, the cell viability after NIR irradiation was evaluated by standard CCK8 method. The equation for CCK8 to test cell viability was as follows

$$\text{Cell viability}\ (\%) = \frac{\text{Abs(test)} - \text{Abs(blank)}}{\text{Abs(control)} - \text{Abs(blank)}} \times 100\%$$

2.8 Animals and OSCC model establishment

All animal experiments were performed in full compliance with guidelines in the Guide for the Care and Use of Laboratory Animals published by the US national Institutes of Health (NIH publication No. 85-23, revised 1985) and were approved by the Ethics Review Board for Animal Studies of Nanjing Stomatological Hospital, Medical School of Nanjing University. Male SPF grade C57BL6 mice (5–7 weeks) were purchased from Model Animal Research Center of Nanjing University. Animal health, including body weight and skin conditions, was monitored twice weekly. Ulceration, a reduction in animal mobility and weight loss was not observed during the experiment. To establish the OSCC allograft model, SCC7 cells (1×10^6 cells in 200 μL PBS) were inoculated subcutaneously in the right leg of C57BL6 mice. Tumor size was measured with calipers every other day, and the equation for tumor volume was as follows

$$\text{Tumor volume} = \frac{(\text{length} \times \text{width} \times \text{width})}{2}$$

where the length was the longest diameter of the tumor and the width was the shortest diameter of the tumor. When the volume of tumors reached 50–100 mm^3, the mice were ready for *in vivo* experiment.

2.9 Biosafety studies *in vivo*

The C57BL6 mice were randomly divided into the experimental group and the control group. The experimental group was injected with SPN-Gd (100 μg/mL, 200 μL) through the tail vein, while the control group mice were untreated and kept in an appropriate environment for one month. The body weight changes of the two groups of mice were recorded every two days. One month later, two groups of mice were anesthetized with 4% chloral hydrate and blood was collected from the eyeball. 20 μL of whole blood was taken for routine blood test. About 800 μL of whole blood was taken and centrifuged at 3,500 rpm for 15 min to obtain serum for blood biochemical examination.

2.10 MR imaging *in vivo*

The mice were under inhalation anesthesia during the *in vivo* MR imaging experiment. Tumor-bearing mice were randomly divided into 4 groups: SPN-Gd (F127-DTPA-Gd = 10, 20, and 30 mg, 200 μL) and Omniscan (Gd^{3+} = 10 mM, 200 μL) were injected via tail vein, respectively. A 9.4T magnetic resonance scanner (Bruker, BioSpec 94/20 USR, Germany) was used. The scanning parameters were set as follows: field of view 32 mm × 32 mm, voxel 256 × 256, resolution 0.125 mm, and slice thickness 0.7 mm. T_1 weighted phase T_R: 800 ms, T_E: 7.5 ms. Firstly, the T_1-weighted axial images of mice without contrast agent were obtained. Then, T_1-weighted axial images of mice were obtained at 24, 48, and 72 h after administration of contrast agent. The signals of tumor-to-background ratio (TBR) on MRI images were calculated and compared among different groups.

2.11 Fluorescence imaging *in vivo*

Tumor-bearing mice were anesthetized by intraperitoneal injection of chloral hydrate (4%, 200 μL). SPN-Gd (100 μg/mL, 200 μL) was injected into tumor-bearing mice via tail vein injection. Subsequent fluorescence images were obtained at 0, 4, 8, 12, 24, 36, 48, 60, and 72 h post-injection using an IVIS Spectral Imaging System (Caliper, IVIS Lumina XR, USA). The fluorescence image acquisition time was 0.1 s, the excitation wavelength was 760 nm, and the emission wavelength was 845 nm.

To explore the biodistribution of the nanoparticle *in vivo*, the mice were sacrificed 72 h after nanoparticles injection, and the major organs (heart, liver, spleen, lung, and kidney) and tumor tissues were collected for fluorescence imaging *in vitro*.

2.12 Photothermal therapy *in vivo*

2.12.1 Photothermal therapy and histological studies

OSCC allograft mice models were established and randomly divided into 4 groups (n = 3): (1) SPN-Gd + PTT group, (2) SPN-Gd group, (3) PTT group, and (4) untreated group. Different treatments were performed for the 4 groups as follows: SPN-Gd + PTT group: SPN-Gd (100 μg/mL, 200 μL) was injected via tail vein. 24 h after injection, the tumors were exposed to 808 nm NIR laser irradiation (1.0 W/cm^2). The temperature of the tumor area was recorded every 10 s, and the infrared thermal images of the mice were taken every 30 s for 5 min. SPN-Gd group: intravenous injection of the same amount of SPN-Gd without laser irradiation. PTT group: intravenous injection of 200 μL normal saline, NIR laser irradiation (1.0 W/cm^2) for 5 min. Untreated group: intravenous injection of 200 μL normal saline, no laser irradiation. The tumor volumes and the weight of mice in each group were measured every 2 days. The tumor volumes were compared among different groups.

After 7 days of treatment, the mice were sacrificed, the tumor tissues, heart, lung, kidney, liver, and spleen of mice in each group were harvested and fixed in 4% formalin. Paraffin embedded sectioning was then performed for hematoxylin and eosin (H&E) staining according to standard protocol, and the images were captured by using a digital microscope.

2.12.2 Survival experiment

In order to evaluate the therapeutic effect, an independent survival experiment was conducted. OSCC mice were also divided into four groups (n = 10): (1) SPN-Gd + PTT group, (2) SPN-Gd group, (3) PTT group, and (4) untreated group. The experiment ended at the 30th day after treatment and the survival curves were drawn.

2.12.3 Blood analysis

OSCC allograft mice were also divided into the above four groups (n = 3). After one day of treatment, blood of mice in each group was taken through the eyeball after anesthesia with 4% chloral hydrate. 20 μL whole blood was taken for blood routine test. About 800 μL whole blood was taken and centrifuged (Holly's, Germany) at 3,500 rpm for 15 min to obtain serum for blood biochemical examination.

Another 100 μL whole blood was stained by a cocktail of fluorescent binding antibody (PerCP anti-mouse CD45 antibody 0.6 μL, FITC anti-mouse CD3 antibody 0.3 μL, APC anti-mouse CD4 antibody 0.6 μL, and PE anti-mouse CD8a antibody 0.3) for 30 min at 4 °C. Following that, the cells were added by 1 mL red blood cell lysis buffer at 4 °C for 15 min and then analyzed with flow cytometry.

2.13 Statistical analysis

GraphPad Prism 8.0 and Image J-Fiji, Flow jo, CaseViewer, RadiAnt DICOM Viewer software was used for data and images analysis. Statistical analysis was performed using T test and variance analysis analysis of variance (ANOVA). The data were listed as mean ± SD, and a value of $P < 0.05$ was considered statistically significant.

3 Results and discussion

3.1 Preparation and characterization of nanoparticles

Pluronic F127, as a biocompatible triblock amphiphilic copolymer composed of poly (ethylene oxide) (PEO) and poly (propylene oxide) (PPO), has been widely used in pharmaceutical manufacturing industry and showed great promise in nanoscience and nanomedicine [19–21]. In this study, a relatively simple synthesized strategy of dual-model imaging and nanotheranostic platform was used. Firstly, F127-DTPA was prepared using an EDC coupling reaction, followed by the synthesis of F127-DTPA-Gd via a chelation reaction and finally PCPDTBT was loaded into the nanoparticles (SPN-Gd).

The molecular equation and flow diagrams for the preparation of nanoparticles F127-DTPA-Gd and SPN-Gd were shown in Fig. 1(a). To improve the diagnosis sensitivity of MRI, metallic MRI contrast agens are used in clinic and the gadolinium (Gd^{3+}) based contrast agents are most widely used because of its advantages in shortening the longitudinal relaxation time (T_1) [22]. In this study, DTPA was firstly grafted onto F127 using an EDC coupling reaction and Gd^{3+} containing amphiphilic copolymer F127-DTPA-Gd was synthesized by a chelation reaction between DTPA and Gd^{3+}. Each batch of products was sampled and the mass percentage of Gd^{3+} in the samples was determined by inductively coupled plasma emission spectrometer. The results showed that the average mass percentage of Gd^{3+} in F127-DTPA-Gd was 1.6% with a yield of 70%. This indicated that the method could synthesize F127-DTPA-Gd efficiently and stably.

PCPDTBT was then co-precipitated with F127-DTPA-Gd using a nanoprecipitation method to form water-soluble nanoparticles, and the formed nanoparticles were termed as SPN-Gd. DLS results showed that the average diameters of F127-DTPA-Gd and SPN-Gd were 36.4 ± 1.4 and 101.3 ± 7.7 nm, respectively (Figs. 2(a) and 2(b)). The diameter of SPN-Gd was larger than that of F127-DTPA-Gd, the encapsulation of PCPDTBT in the nanoparticles would appear to increase the size of nanoparticles. The TEM showed SPN-Gd to be dispersed and spherical particles (Fig. 2(c)). The average particle size of both nanoparticles in PBS solution did not change significantly even after storage for 30 days in PBS (pH = 7.4), indicating their good physiological stabilities (Fig. 2(d)).

In this study, the longitudinal relaxation rate (r_1) and transverse relaxation rate (r_2) of SPN-Gd at different Gd^{3+} concentrations were measured and calculated on 9.4T magnetic resonance with F127-DTPA-Gd and Omniscan as controls (Fig. 3). The results showed that both F127-DTPA-Gd and SPN-Gd had higher r_1 and r_2 than Omniscan, while SPN-Gd has the highest r_1 and r_2. The higher relaxation rate of nanoparticles compared to Omniscan may be related to the increased molecular weight. It is known that relaxation rate (r) is an important characteristic of MR contrast agents [22, 23]. The higher relaxation rate, the stronger signal change by contrast agent. The high r_1 and r_2 of SPN-Gd suggested it could provide better contrast differences between normal tissues

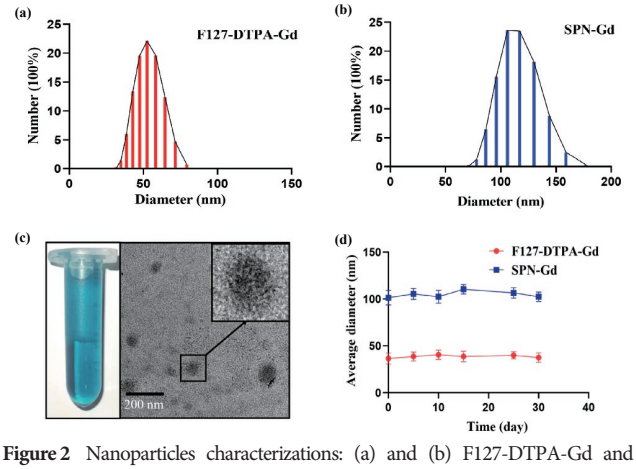

Figure 2 Nanoparticles characterizations: (a) and (b) F127-DTPA-Gd and SPN-Gd particle size measured by DLS; (c) representative TEM images of SPN-Gd; and (d) the stability of F127-DTPA-Gd and SPN-Gd.

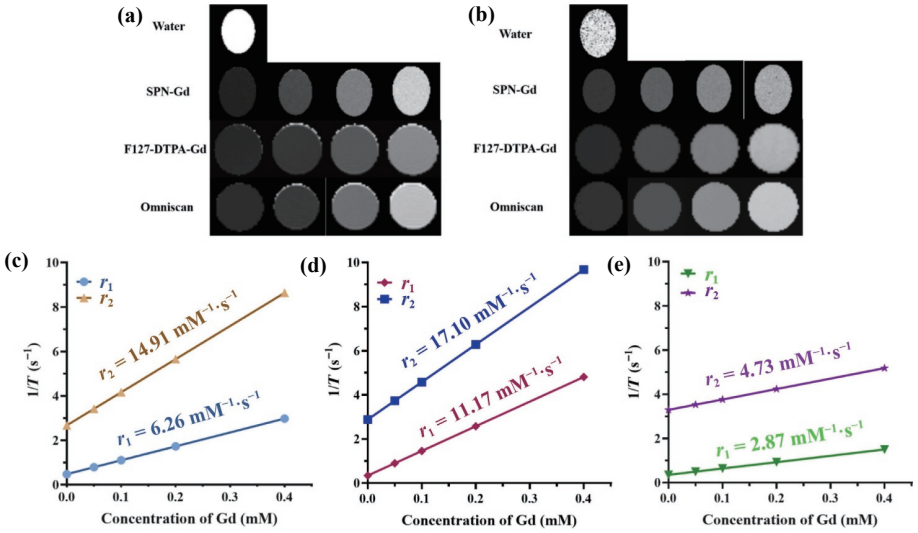

Figure 3 *In vitro* magnetic resonance relaxation rate test of nanoparticles: (a) and (b) T_1 mapping and T_2 mapping images of SPN-Gd, F127-DTPA-Gd, and Omniscan under 9.4T MRI; (c)–(e) the longitudinal relaxation rate (r_1) and transverse relaxation rate (r_2) of F127-DTPA-Gd, SPN-Gd, and Omniscan.

and tumors for *in vivo* usage.

The optical properties of SPN-Gd were then investigated. As shown in Fig. 4(a), SPN-Gd had two absorption peaks between 300 and 900 nm and the maximum absorption peak was near 690 nm. The excitation spectrum showed that the maximum excitation wavelength of SPN-Gd was near 833 nm (Fig. 4(b)). Compared with PCPDTBT (λ_{max} = 760 nm), the emission spectrum of SPN-Gd (λ_{max} = 833 nm) exhibited a degree of red shift. This suggested that the block copolymers have a certain influence of the emission band of PCPDTBT, but it was still within the fluorescence range of NIR-I (700–900 nm) [24–26]. The use of F127-DTPA-Gd as a nanocarrier did not significantly alter the optical properties of PCPDTBT. The separation of absorption and emission spectra could greatly reduce the energy levels of background spontaneous fluorescence and scattering induced luminescence and improve the quality of near-infrared fluorescence imaging. The content of PCPDTBT in SPN-Gd was calculated to have the EE was about 82.2%. And the photostability of SPN-Gd and ICG showed that the maximum absorption peak of ICG decreased rapidly, while SPN-Gd almost the same within 30 min (Fig. 4(c)), indicating that SPN-Gd had good photostability. The photothermal performance of SPN-Gd was also studied. After irradiation with NIR light, the temperature of SPN-Gd rose rapidly to 60 °C in a short time. The temperature of SPN-Gd was positively correlated with the intensity of NIR laser and the concentration of SPN-Gd, indicating that SPN-Gd had good power and concentration dependence (Figs. 4(d) and 4(e)). The heating and cooling curve of SPN-Gd remained stable after three irradiations, indicating that the photothermal conversion ability of SPN-Gd was stable (Fig. 4(f)).

3.2 Cellular uptake studies

The uptake of nanoparticles by tumor cells was one of the prerequisites for our experiment. Figure 5 showed the uptake of SPN-Gd by tumor cells observed with laser confocal microscope. The SPN-Gd in the tumor cells was shown as green fluorescence, while the nuclei labelled by DAPI showed blue fluorescence. The results showed that after 30 min of co-incubation, SPN-Gd was close to or around the cell membrane. After 2 h, it could be observed that SPN-Gd mainly distributed in the cytoplasm. These results suggested that SPN-Gd could be uptaken by tumor cells through cell membrane and concentrated in the cytoplasm. During this process, there was no significant change in the shape and size of the cells. It further suggested that these nanoparticles could effectively penetrate the cell membrane barrier with low

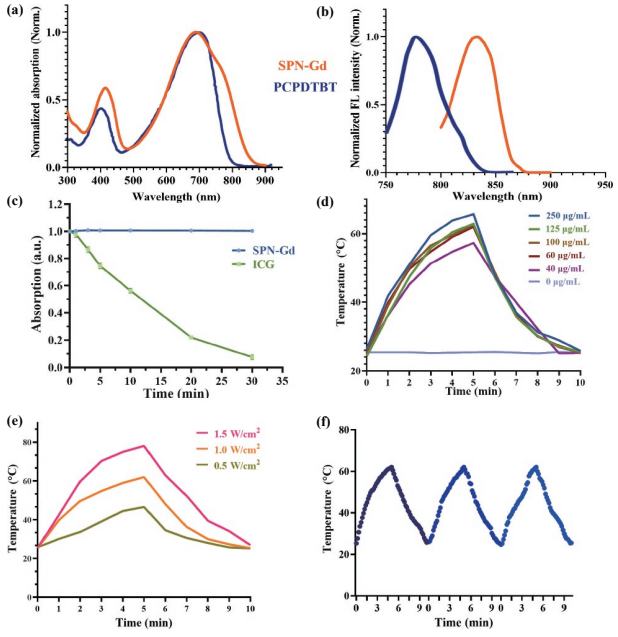

Figure 4 *In vitro* optical properties of nanoparticles: (a) and (b) normalized absorption spectra and fluorescence emission spectra of PCPDTBT and SPN-Gd; (c) photostability of SPN-Gd and ICG; (d) concentration dependence of SPN-Gd temperature; (e) power dependence of SPN-Gd temperature; and (f) heating and cooling curve of SPN-Gd.

toxicity and good biocompatibility.

3.3 Cell viability and apoptosis assays *in vitro*

The growth of SCC7 cells exposed to F127-DTPA-Gd and SPN-Gd was measured by CCK8 cell recording method. SPN-Gd showed overall good biocompatibility with NIH 3T3 cells (Fig. 6(a)). F127-DTPA-Gd, SPN-Gd, and Omniscan showed almost no cytotoxicity to OSCC cells without light irradiation, indicating their good biocompatibility (Fig. 6(b)). In addition, photothermal therapy is to convert light energy into heat energy, which raises the local temperature of target cells, leading to protein degeneration and cell membrane destruction [27]. Therefore, in another group of CCK8 cytotoxicity test, different concentrations of PCPDTBT had no significant effect on the cell viability of SCC7 cells without NIR laser irradiation ($P > 0.05$). After incubation for 12 and 24 h, the cell viability of SCC7 cells decreased significantly with NIR laser irradiation ($P < 0.05$), and the cell viability for the highest

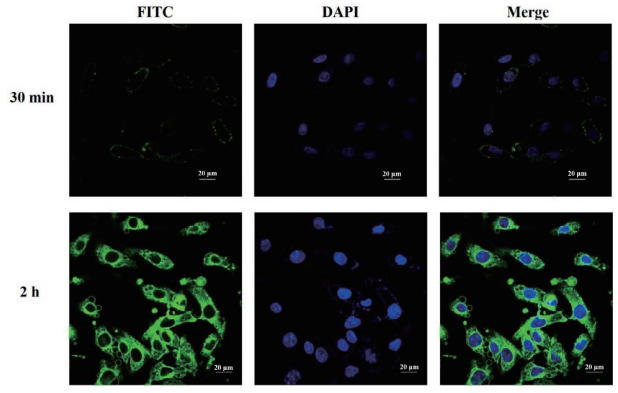

Figure 5 Cellular uptake of SPN-Gd by SCC7 cells for 30 min and 2 h (scale bar: 20 μm). Green: FITC; blue: DAPI. After 30 min of co-incubation, the green fluorescence signal was mainly distributed close to or around the cell membrane. After 2 h, the green fluorescence signal was mainly distributed in the cytoplasm.

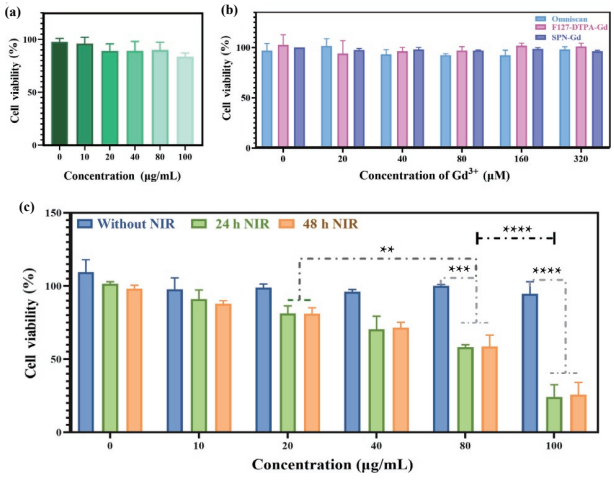

Figure 6 Nanoparticles cytotoxicity assay: the cytotoxicity of SPN-Gd with different concentrations and the effect of photothermal effect on (a) NIH 3T3 cells and (c) cancer cells; (b) cytotoxicity of SPN-Gd, F127-DTPA-Gd, and Omniscan based on Gd^{3+} concentration on cancer cells.

concentration of SPN-Gd (100 μg/mL) was 24.2% after 24 h (Fig. 6(c)). This indicated that SPN-Gd could inhibit OSCC cell growth and the photothermal effect enhanced at higher SPN-Gd concentration.

3.4 Biosafety studies *in vivo*

In the biosafety study *in vivo*, the body weight of the mice in the experimental and control groups increased slightly over a period of one month (Fig. 7(a)), and there were no significant differences between the two groups in blood routine and blood biochemical tests (Figs. 7(b) and 7(c)). The results demonstrated that SPN-Gd had good biological safety, and no effect on physical skills and liver and kidney functions of experimental mice.

3.5 MR/fluorescence dual-modal imaging *in vivo*

SPN-Gd and Omniscan were injected intravenously as T_1 positive contrast agents for *in vivo* MR imaging. Contrast images were obtained 24, 48, and 72 h after injection (Fig. 8(c)). The TBR was calculated and used as quantitative indexes for evaluation. Figures 8(a) and 8(b) showed that TBR of SPN-Gds (20 mg) increased gradually after injection, and maintained from 24 to 72 h after injection; however, the TBR of Omniscan reached maximum at

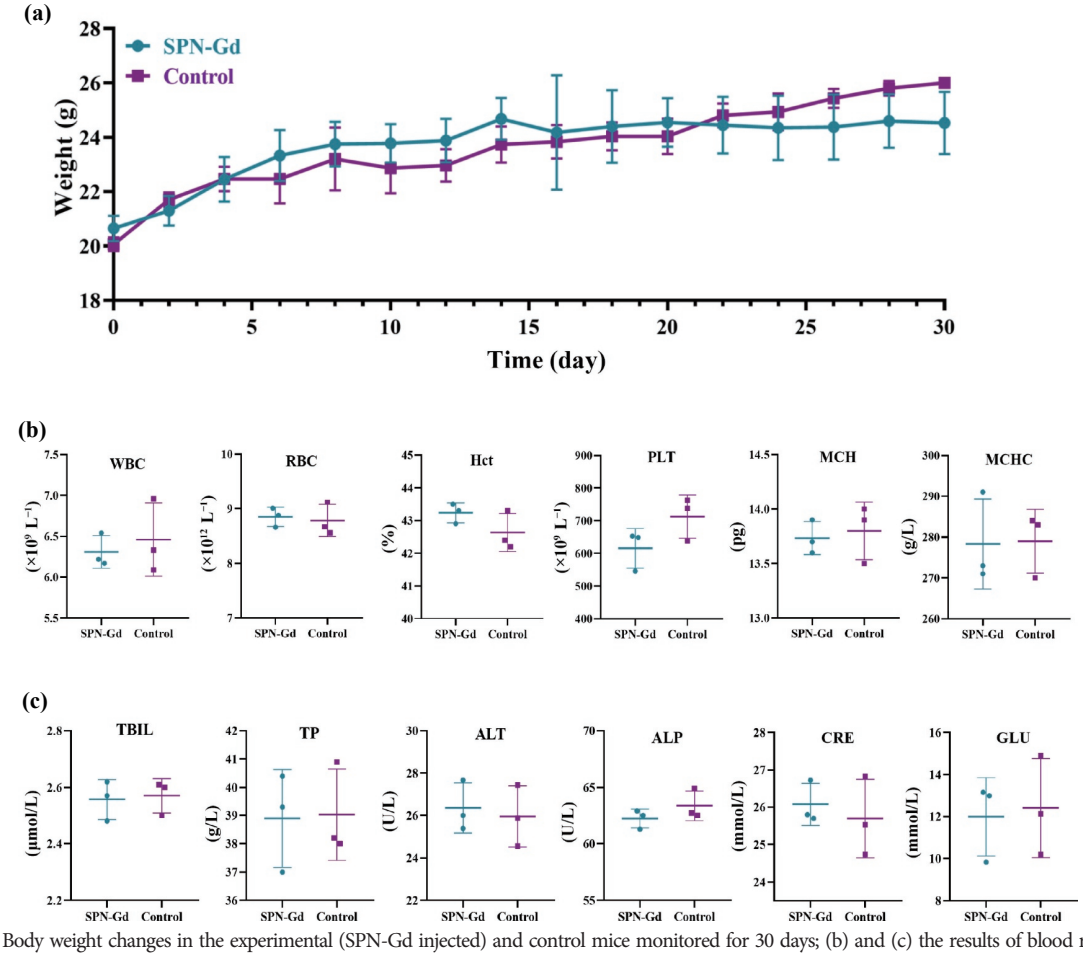

Figure 7 (a) Body weight changes in the experimental (SPN-Gd injected) and control mice monitored for 30 days; (b) and (c) the results of blood routine test and blood biochemical test of the experimental and control group of mice.

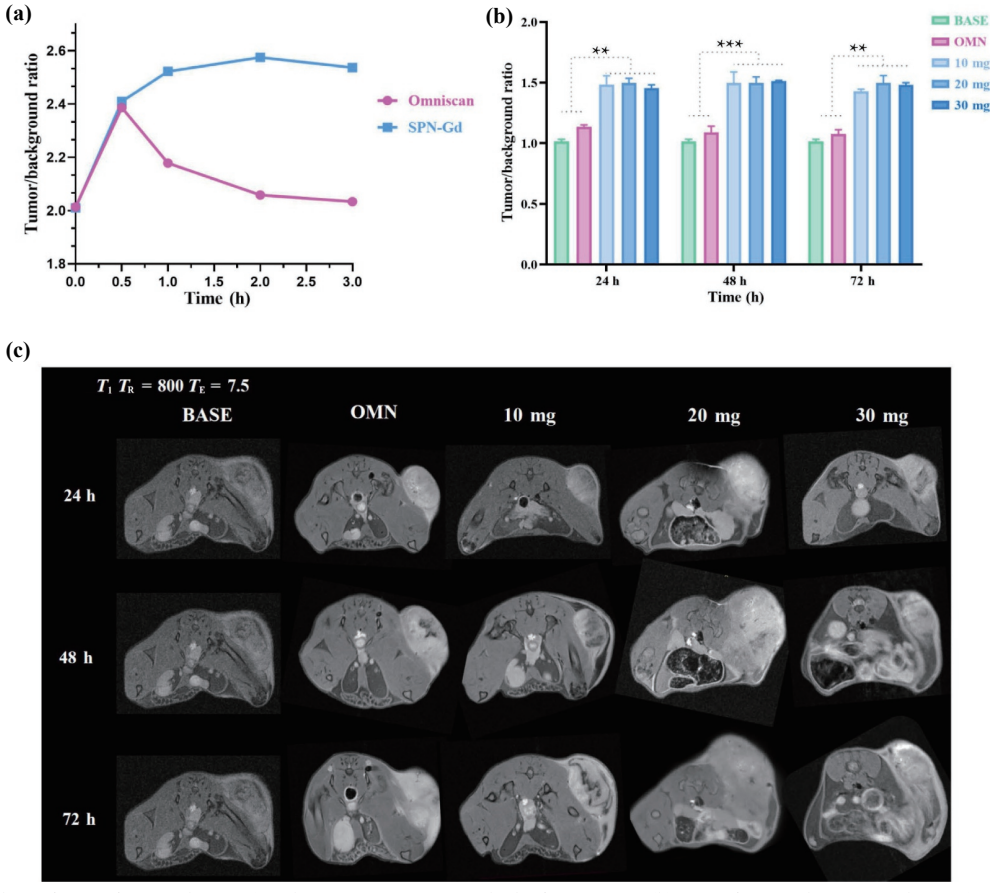

Figure 8 (a) Line chart of TBR of SPN-Gd (20 mg) and Omniscan 0.5, 1, 2, and 3 h after injection; (b) TBR of SPN-Gd (10, 20, and 30 mg) and Omniscan 24, 48, and 72 h after injection; and (c) T_1 weighted MR images of tumor-bearing mice 24, 48, and 72 h after injection with SPN-Gd and Omniscan as contrast agent.

30 min, decreased gradually from 30 min and back to almost the baseline at 3 h. Figure 8(b) showed that the TBR of SPN-Gds were higher than that of Omniscan at 24, 48, and 72 h ($p < 0.05$), and there were no significant differences among different concentrations of SPN-Gd, which suggested that 10 mg SPN-Gd was sufficient for *in vivo* usage of mice model. The *in vivo* experiment proved that SPN-Gd, as a macromolecular contrast agent, had good proton relaxation enhancement effect and long retention time, which also indicated the tumor specificity of our SPN-Gd nanoparticles.

After intravenous injection of nanoparticles, fluorescence signals were observed at the tumor site in the mice model; the fluorescence signal gradually increased, reaching a maximum at 24 h, and was maintained from 24 to 72 h (Figs. 9(a) and 9(c)). The high fluorescence signal at the tumour site confirmed the aggregation of SPN-Gd in the tumor with a long retention time, which was consistent with *in vivo* MRI imaging. Then the NIR images of SPN-Gd were compared with ICG (a widely used NIR agent in clinic), the results showed that the fluorescence signal of SPN-Gd was higher and longer than ICG, indicating the advantages used as an *in vivo* NIR agent (Fig. 9(c)). The maximum fluorescence signal of SPN-Gd at 24 h also suggested that PTT should be performed 24 h after injection of SPN-Gd. Moreover, *ex vivo* biodistribution for SPN-Gd was acquired by fluorescence imaging at 72 h post-injection. Liver had the highest fluorescence signal, which followed by tumor, spleen, and other major organs (Figs. 9(d) and 9(e)). These data showed that SPN-Gd could passively accumulate into tumor and successfully detect tumors both by MRI and fluorescence images.

3.6 Photothermal therapy *in vivo*

The advantages of PTT in the treatment of OSCC are as follows: (1) Less invasive and less side effects, this is beneficial to subsequent maxillofacial defects repair; (2) tumor-targeted; (3) high clinic operability; and (4) MR/fluorescence dual-modal imaging-guided PTT with high accuracy. To evaluate the *in vivo* photothermal antitumor effect, SPN-Gd was intravenous injected, and the temperature of the tumor area was recorded (Figs. 10(a) and 10(b)). It could be seen that the tumor temperature rose gradually and reached a maximum temperature of 52 °C after 5 min, demonstrating the good photothermal conversion ability of SPN-Gd (Fig. 10(c)). Compared with other control groups, the tumor in SPN-Gd + PTT group had slowest growth, and the tumor volume in SPN-Gd + PTT group was significantly smaller than that in untreated group at the end of experiment ($P < 0.05$), which indicated that SPN-Gd guided PTT could inhibit the tumor growth (Fig. 10(d)). For all the groups, the body weight of mice increased smoothly, showing almost no side effect of treatments (Fig. 10(e)). The survival experiment showed the mice in untreated group began to die 14 days after tumor implantation, while nearly half of the mice in SPN-Gd + PTT group survived at the end of the experiment ($P < 0.05$), indicating the effectiveness of our treatment (Fig. 10(f)). According to histological analysis, compared with the denser tumor cells in other groups, the tumor cells in the treatment group were sparse, separated, and less atypica; no cellular abnormalities were observed in the major organs of all mice, which confirmed that SPN-Gd nanoparticles had no obvious toxicity (Fig. 11).

In addition, there were no significant differences of blood routine test and blood biochemical test results among the four groups ($P > 0.05$), indicating that the nanoparticles had good biosafety (Fig. 12(a)).

In this study, we further evaluated the immune activation by SPN-Gd-guided PTT with flow cytometry analysis. The content of

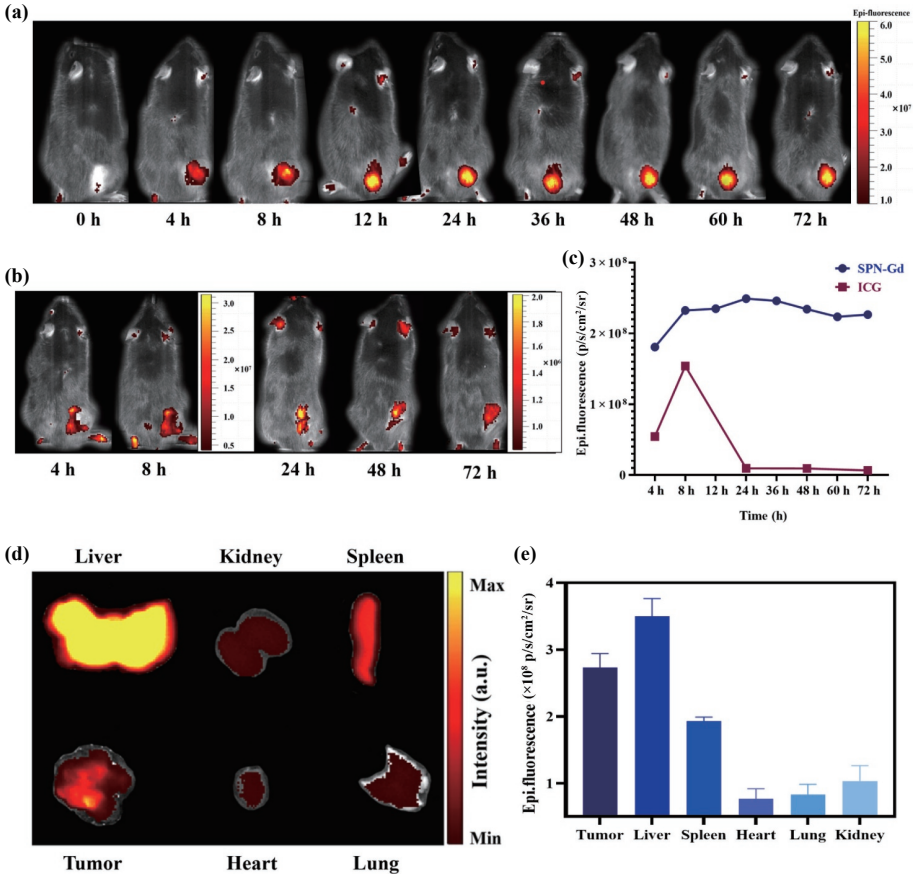

Figure 9 (a) Fluorescence images at different time points after injection of SPN-Gd; (b) fluorescence images at different time points after ICG injection; (c) comparison of fluorescence signal intensity between SPN-Gd and ICG at different time points; and (d) and (e) *in vitro* fluorescence signal intensity of main organs and tumors 72 h after injection of SPN-Gd.

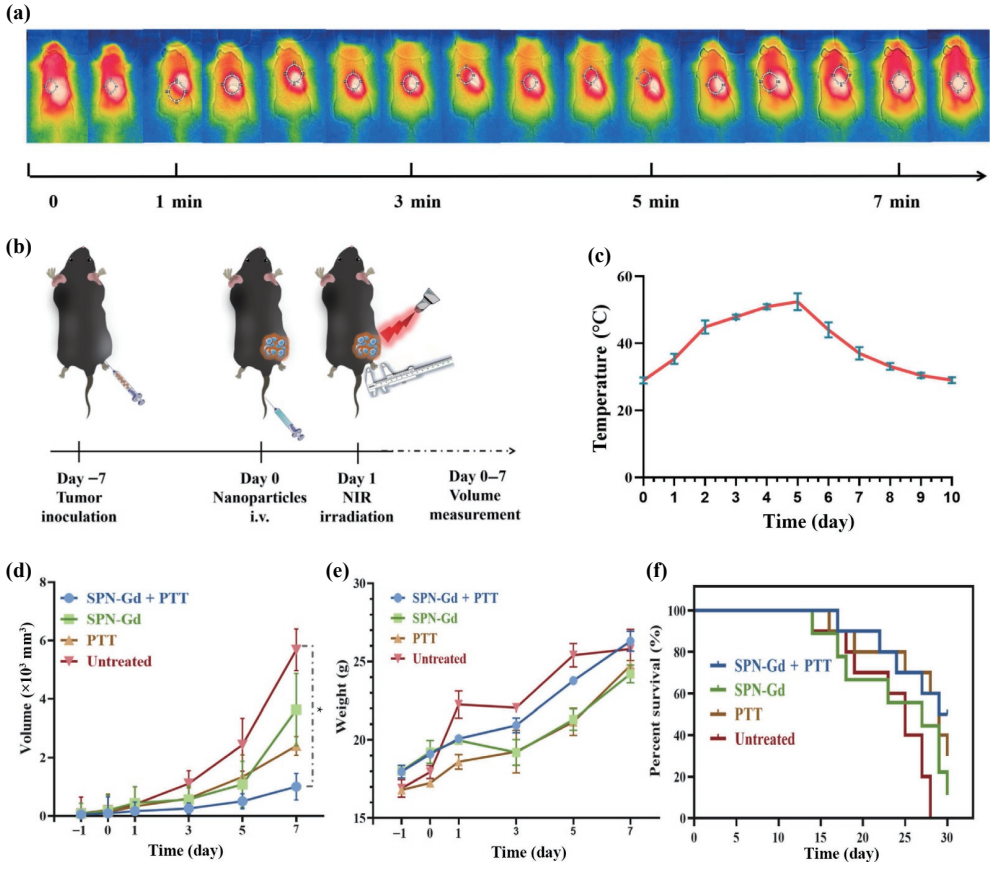

Figure 10 *In vivo* photothermal therapy: (a) infrared thermogram showing the change of mouse body temperature after irradiation: the high temperature area (the white area) gradually concentrated in the tumor area after irradiation (0 to 5 min), and gradually dispersed after irradiation stopped (5 to 7 min); (b) schematic illustration of PTT in tumor models.; (c) local temperature changes after NIR irradiation; (d) tumor growth curves and (e) body weight changes of tumor bearing mice after different treatments; and (f) survival curves of tumor bearing mice.

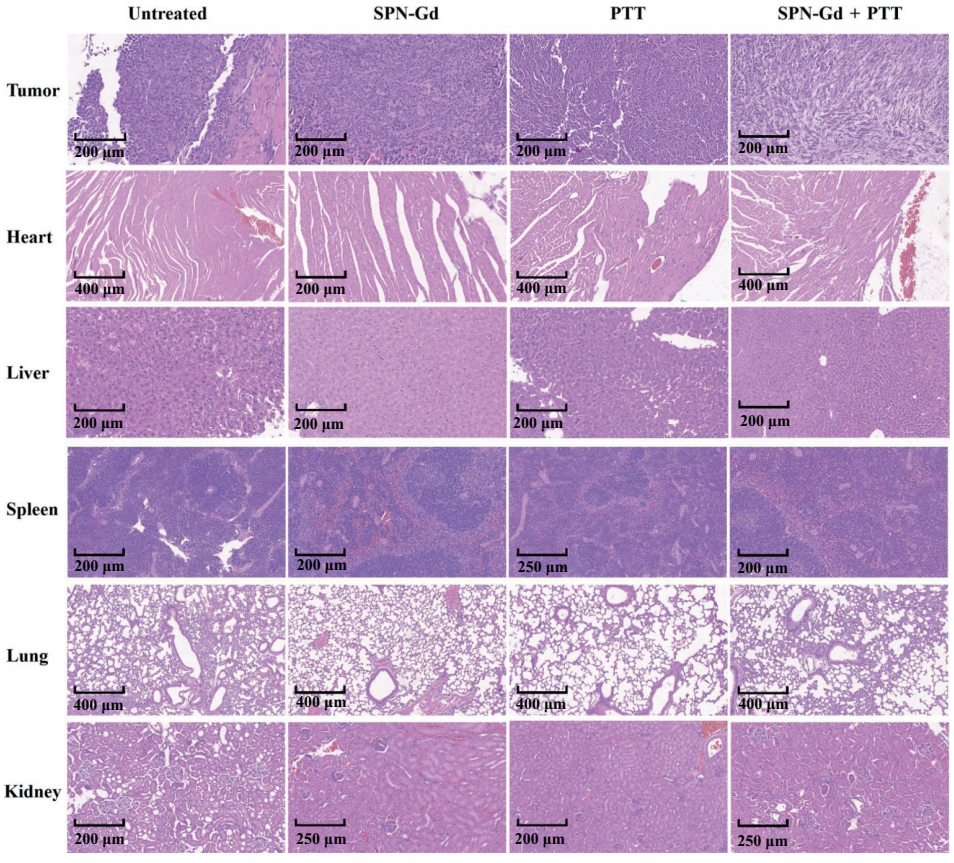

Figure 11 H&E staining of major organs from tumor bearing mice after different treatments.

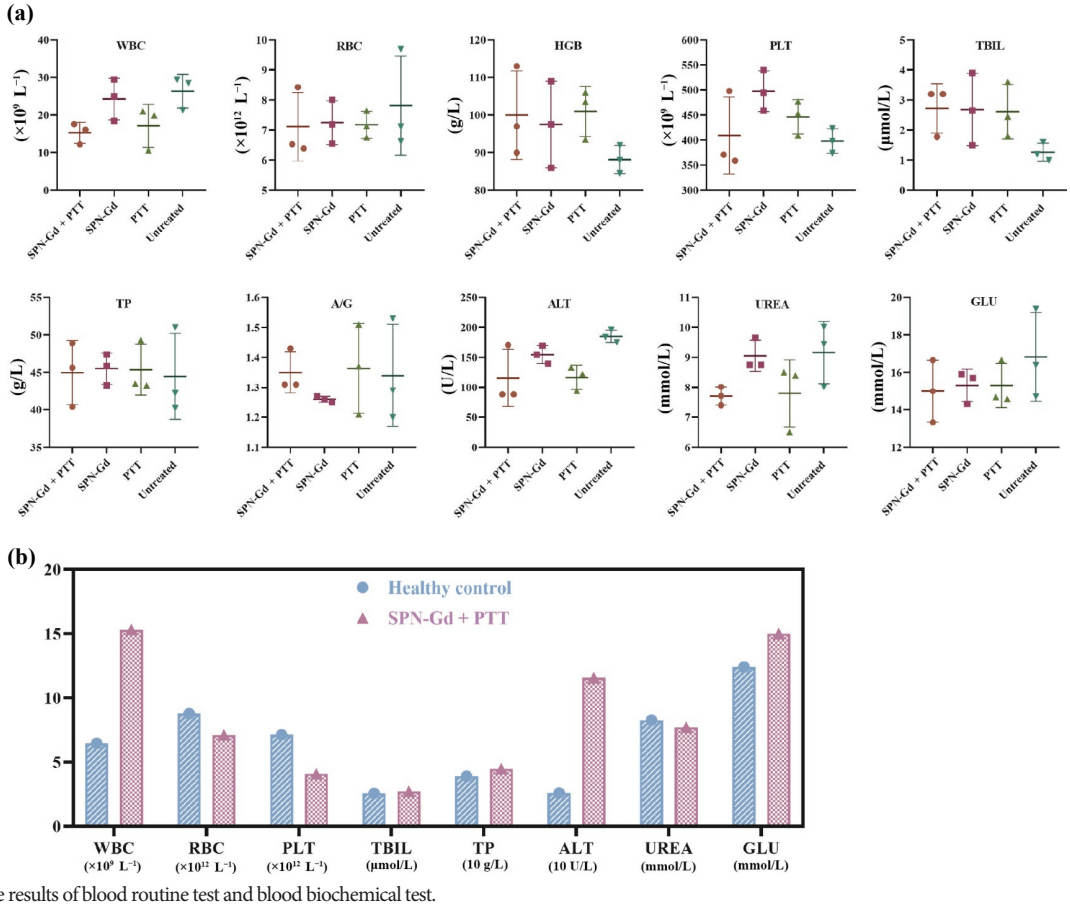

Figure 12 The results of blood routine test and blood biochemical test.

$CD3^+$ T cells in the blood of SPN-Gd + PTT group was higher than those of other control groups (Fig. 13(b)). Moreover, the proportion of $CD4^+$ T cells and $CD8^+$ T cells in SPN-Gd + PTT group was higher than other groups (Figs. 13(c)–13(e)), indicating that SPN-Gd-guided PTT could cause specific T activation. According to the previuos studies, some anthracyclines, DNA

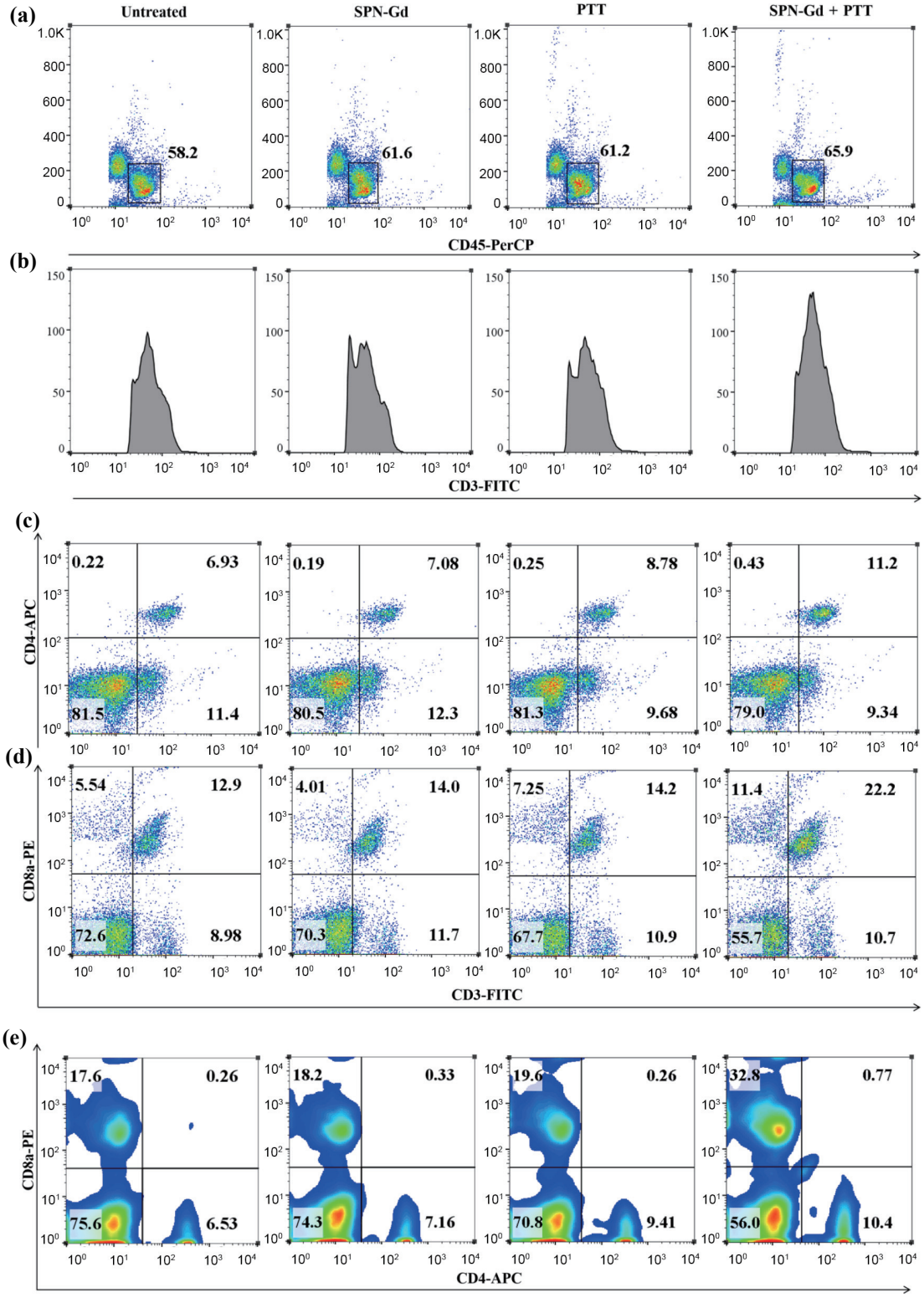

Figure 13 Flow cytometry analysis of blood immune cells of mice after different treatments: (a) proportion of CD45 positive leukocytes in blood; (b) $CD3^+$ cells quantity analysis; and (c)–(e) the proportion of $CD4^+$ and $CD8^+$ T cells gated by $CD3^+$ cells in blood.

damaging agents and other chemotherapeutic drugs, radiotherapy, radiation, phototherapy, or multiple treatment synergistic therapy can induce immunogenic cell death (ICD) of tumor cells [28–32]. Once ICD has occured, it can release a variety of signals. Among them, high migration rate protein B1 can promote the combination of dendritic cells and tumor cells [28, 33], which facilitate the induction of specific T-cell anti-tumour immunity in the organism [28, 34]. In some cases of breast cancer and colon cancer, the proportion of cytotoxic T cells and regulatory T cells is increased after induction of ICD, and the prognosis of anti-cancer therapy is good [31, 35–38]. Therefore, based on the previous literatures as well as our experimental results, it was hypothesized that the ICD of cancer cells induced by PTT successfully enhanced the activation of anti-tumor immunity, which might contribute to the efficacy and prognosis of PTT in the treatment of OSCC.

4 Conclusions

In summary, we have designed and prepared SPN-Gd for MR/fluorescence dual-modal imaging and imaging-guided PTT.

The nanoparticles are composed of a NIR absorption semiconductor polymer (PCPDTBT) served as fluorescence signal source and PTA and a gadolinium-grafted tri block amphiphilic copolymer (F127-DTPA-Gd) served as MRI contrast agent and nanocarrier. The experiments *in vivo* showed that SPN-Gd could be used as an MRI contrast agent and optical image agent with a long retention time, and it had a significant inhibiting effect on tumors of OSCC mice model through PTT. Our study thus provides a simple nanotheranostic platform composed of two components for efficient MR/fluorescence dual-modal imaging-guided PTT.

Acknowledgements

This work was supported by the National Natural Science Foundation of China (Nos. 82201135, 22174070, and 61905122), Nanjing Clinical Research Center for Oral Diseases (No. 2019060009), General project of Jiangsu Provincial Health Commission (No. M2021077), Scientific research fund of Jiangsu Medical Association (No. SYH-3201150-0007(2021002)), and the Natural Science Foundation of Jiangsu Province (No. BK20190735).

References

[1] Chamoli, A.; Gosavi, A. S.; Shirwadkar, U. P.; Wangdale, K. V.; Behera, S. K.; Kurrey, N. K.; Kalia, K.; Mandoli, A. Overview of oral cavity squamous cell carcinoma: Risk factors, mechanisms, and diagnostics. *Oral Oncol.* **2021**, *121*, 105451.

[2] Ishida, K.; Nakashima, T.; Shibata, T.; Hara, A.; Tomita, H. Role of the DEK oncogene in the development of squamous cell carcinoma. *Int. J. Clin. Oncol.* **2020**, *25*, 1563–1569.

[3] Sung, H.; Ferlay, J.; Siegel, R. L.; Laversanne, M.; Soerjomataram, I.; Jemal, A.; Bray, F. Global cancer statistics 2020: GLOBOCAN estimates of incidence and mortality worldwide for 36 cancers in 185 countries. *CA Cancer J. Clin.* **2021**, *71*, 209–249.

[4] Gao, A. T.; Pan, X.; Yang, X. D.; Lin, Z. T. Predictive factors in the treatment of oral squamous cell carcinoma using PD-1/PD-L1 inhibitors. *Invest. New Drugs* **2021**, *39*, 1132–1138.

[5] Han, Z.; Li, Y. J.; Roelle, S.; Zhou, Z. X.; Liu, Y. C.; Sabatelle, R.; DeSanto, A.; Yu, X.; Zhu, H.; Magi-Galluzzi, C. et al. Targeted contrast agent specific to an oncoprotein in tumor microenvironment with the potential for detection and risk stratification of prostate cancer with MRI. *Bioconjug. Chem.* **2017**, *28*, 1031–1040.

[6] Kim, H. K.; Lee, G. H.; Chang, Y. M. Gadolinium as an MRI contrast agent. *Future Med. Chem.* **2018**, *10*, 639–661.

[7] Morana, G.;Cugini, C.;Scatto, G.;Zanato, R.;Fusaro, M.; Dorigo, A. Use of contrast agents in oncological imaging: magnetic resonance imaging. *Cancer Imaging* **2013**, *13*, 350–359.

[8] Shirazi, A. N.; Park, S. E.; Rad, S.; Baloyan, L.; Mandal, D.; Sajid, M. I.; Hall, R.; Lohan, S.; Zoghebi, K.; Parang, K. et al. Cyclic peptide-gadolinium nanoparticles for enhanced intracellular delivery. *Pharmaceutics* **2020**, *12*, 792.

[9] Xin, X. Y.; Sha, H. Z.; Shen, J. T.; Zhang, B.; Zhu, B.; Liu, B. R. Coupling Gd-DTPA with a bispecific, recombinant protein anti-EGFR-iRGD complex improves tumor targeting in MRI. *Oncol. Rep.* **2016**, *35*, 3227–3235.

[10] Usman, M. S.; Hussein, M. Z.; Fakurazi, S.; Saad, F. F. A. Gadolinium-based layered double hydroxide and graphene oxide nano-carriers for magnetic resonance imaging and drug delivery. *Chem. Cent. J.* **2017**, *11*, 47.

[11] Ji, Y. Y.; Jones, C.; Baek, Y.; Park, G. K.; Kashiwagi, S.; Choi, H. S. Near-infrared fluorescence imaging in immunotherapy. *Adv. Drug Deliv. Rev.* **2020**, *167*, 121–134.

[12] Pan, X.; Gao, A. T.; Lin, Z. T. Fluorescence imaging of tumor immune contexture in immune checkpoint blockade therapy. *Int. Immunopharmacol.* **2022**, *106*, 108617.

[13] Yan, R. Q.; Hu, Y. X.; Liu, F.; Wei, S. X.; Fang, D. Q.; Shuhendler, A. J.; Liu, H.; Chen, H. Y.; Ye, D. J. Activatable NIR fluorescence/MRI bimodal probes for *in vivo* imaging by enzyme-mediated fluorogenic reaction and self-assembly. *J. Am. Chem. Soc.* **2019**, *141*, 10331–10341.

[14] Feng, L. H.; Zhu, C. L.; Yuan, H. X.; Liu, L. B.; Lv, F. T.; Wang, S. Conjugated polymernanoparticles: Preparation, properties, functionalization and biological applications. *Chem. Soc. Rev.* **2013**, *42*, 6620–6633.

[15] Zhou, W.; Chen, Y.; Zhang, Y. T.; Xin, X. Y.; Li, R. T.; Xie, C.; Fan, Q. L. Iodine-rich semiconducting polymer nanoparticles for CT/fluorescence dual-modal imaging-guided enhanced photodynamic therapy. *Small* **2020**, *16*, 1905641.

[16] Zhu, C. L.; Liu, L. B.; Yang, Q.; Lv, F. T.; Wang, S. Water-soluble conjugated polymers for imaging, diagnosis, and therapy. *Chem. Rev.* **2012**, *112*, 4687–4735.

[17] Zhen, X.; Xie, C.; Pu, K. Y. Temperature-correlated afterglow of a semiconducting polymer nanococktail for imaging-guided photothermal therapy. *Angew. Chem., Int. Ed.* **2018**, *57*, 3938–3942.

[18] Hu, J. J.; Cheng, Y. J.; Zhang, X. Z. Recent advances in nanomaterials for enhanced photothermal therapy of tumors. *Nanoscale* **2018**, *10*, 22657–22672.

[19] Herzberger, J.; Niederer, K.; Pohlit, H.; Seiwert, J.; Worm, M.; Wurm, F. R.; Frey, H. Polymerization of ethylene oxide, propylene oxide, and other alkylene oxides: Synthesis, novel polymer architectures, and bioconjugation. *Chem. Rev.* **2016**, *116*, 2170–2243.

[20] Naruphontjirakul, P.; Viravaidya-Pasuwat, K. Development of anti-HER2-targeted doxorubicin-core–shell chitosan nanoparticles for the treatment of human breast cancer. *Int. J. Nanomed.* **2019**, *14*, 4105–4121.

[21] Vu-Quang, H.; Vinding, M. S.; Nielsen, T.; Ullisch, M. G.; Nielsen, N. C.; Nguyen, D. T.; Kjems, J. Pluronic F127-folate coated super paramagenic iron oxide nanoparticles as contrast agent for cancer diagnosis in magnetic resonance imaging. *Polymers* **2019**, *11*, 743.

[22] Xiao, Y. D.; Paudel, R.; Liu, J.; Ma, C.; Zhang, Z. S.; Zhou, S. K. MRI contrast agents: Classification and application (review). *Int. J. Mol. Med.* **2016**, *38*, 1319–1326.

[23] Chaabane, L.; Tei, L.; Miragoli, L.; Lattuada, L.; von Wronski, M.; Uggeri, F.; Lorusso, V.; Aime, S. *In vivo* MR imaging of fibrin in a neuroblastoma tumor model by means of a targeting Gd-containing peptide. *Mol. Imaging Biol.* **2015**, *17*, 819–828.

[24] Abelha, T. F.; Neumann, P. R.; Holthof, J.; Dreiss, C. A.; Alexander, C.; Green, M.; Dailey, L. A. Low molecular weight PEG-PLGA polymers provide a superior matrix for conjugated polymer nanoparticles in terms of physicochemical properties, biocompatibility and optical/photoacoustic performance. *J. Mater. Chem. B* **2019**, *7*, 5115–5124.

[25] Yoon, J.; Kwag, J.; Shin, T. J.; Park, J.; Lee, Y. M.; Lee, Y.; Park, J.; Heo, J.; Joo, C.; Park, T. J. et al. Nanoparticles of conjugated polymers prepared from phase-separated films of phospholipids and polymers for biomedical applications. *Adv. Mater.* **2014**, *26*, 4559–4564.

[26] Wu, C. F.; Bull, B.; Szymanski, C.; Christensen, K.; McNeill, J. Multicolor conjugated polymer dots for biological fluorescence imaging. *ACS Nano* **2008**, *2*, 2415–2423.

[27] Wang, Y. F.; Meng, H. M.; Li, Z. H. Near-infrared inorganic nanomaterial-based nanosystems for photothermal therapy. *Nanoscale* **2021**, *13*, 8751–8772.

[28] Park, S. J.; Ye, W. D.; Xiao, R.; Silvin, C.; Padget, M.; Hodge, J. W.; van Waes, C.; Schmitt, N. C. Cisplatin and oxaliplatin induce similar immunogenic changes in preclinical models of head and neck cancer. *Oral Oncol.* **2019**, *95*, 127–135.

[29] Gupta, G.; Borglum, K.; Chen, H. X. Immunogenic cell death: A step ahead of autophagy in cancer therapy. *J. Cancer Immunol. (Wilmington)* **2021**, *3*, 47–59.

[30] Sweeney, E. E.; Cano-Mejia, J.; Fernandes, R. Photothermal therapy generates a thermal window of immunogenic cell death in neuroblastoma. *Small* **2018**, *14*, 1800678.

[31] Yu, Y. J.; Li, J.; Song, B. Y.; Ma, Z.; Zhang, Y. F.; Sun, H. N.; Wei, X. S.; Bai, Y. Y.; Lu, X. G.; Zhang, P. et al. Polymeric PD-L1 blockade nanoparticles for cancer photothermal-immunotherapy.

Biomaterials **2022**, *280*, 121312.

[32] Ruan, H. T.; Bu, L. L.; Hu, Q. Y.; Cheng, H.; Lu, W. Y.; Gu, Z. Strategies of combination drug delivery for immune checkpoint blockades. *Adv. Healthc. Mater.* **2019**, *8*, 1801099.

[33] Aoto, K.; Mimura, K.; Okayama, H.; Saito, M.; Chida, S.; Noda, M.; Nakajima, T.; Saito, K.; Abe, N.; Ohki, S. et al. Immunogenic tumor cell death induced by chemotherapy in patients with breast cancer and esophageal squamous cell carcinoma. *Oncol. Rep.* **2018**, *39*, 151–159.

[34] Fabian, K. P.; Wolfson, B.; Hodge, J. W. From immunogenic cell death to immunogenic modulation: Select chemotherapy regimens induce a spectrum of immune-enhancing activities in the tumor microenvironment. *Front. Oncol.* **2021**, *11*, 728018.

[35] Xie, Q.; Li, Z.; Liu, Y.; Zhang, D. W.; Su, M.; Niitsu, H.; Lu, Y. Y.; Coffey, R. J.; Bai, M. F. Translocator protein-targeted photodynamic therapy for direct and abscopal immunogenic cell death in colorectal cancer. *Acta Biomater.* **2021**, *134*, 716–729.

[36] Ruan, H.; Leibowitz, B. J.; Zhang, L.; Yu, J. Immunogenic cell death in colon cancer prevention and therapy. *Mol. Carcinog.* **2020**, *59*, 783–793.

[37] Heshmati Aghda, N.; Abdulsahib, S. M.; Severson, C.; Lara, E. J.; Torres Hurtado, S.; Yildiz, T.; Castillo, J. A.; Tunnell, J. W.; Betancourt, T. Induction of immunogenic cell death of cancer cells through nanoparticle-mediated dual chemotherapy and photothermal therapy. *Int. J. Pharm.* **2020**, *589*, 119787.

[38] Sistigu, A.; Yamazaki, T.; Vacchelli, E.; Chaba, K.; Enot, D. P.; Adam, J.; Vitale, I.; Goubar, A.; Baracco, E. E.; Remédios, C. et al. Cancer cell-autonomous contribution of type I interferon signaling to the efficacy of chemotherapy. *Nat. Med.* **2014**, *20*, 1301–1309.